



Contents lists available at ScienceDirect

Journal of King Saud University – Science

journal homepage: www.sciencedirect.com



Original article

Phytochemistry, biological activities and in silico molecular docking studies of *Oxalis pes-caprae* L. compounds against SARS-CoV-2Farhat Gul^a, Ilham Khan^a, Javed Iqbal^b, Banzeer Ahsan Abbasi^b, Amir Shahbaz^a, Raffaele Capasso^c, Itzel Amaro-Estrada^{e,*}, Yousef A. Bin Jordan^d, Raquel Cossio-Bayugar^e, Tariq Mahmood^{a,f,*}^a Department of Plant Sciences, Faculty of Biological Sciences, Quaid-i-Azam University, Islamabad 45320, Pakistan^b Department of Botany, Bacha Khan University, Charsadda, Khyber Pakhtunkhwa, Pakistan^c Department of Agricultural Sciences, University of Naples Federico II, Portici (Naples), Italy^d Department of Pharmaceutics, College of Pharmacy, King Saud University, Riyadh 11451, Saudi Arabia^e Centro Nacional de Investigación Disciplinaria en Salud Animal e Inocuidad, INIFAP, Km 11 Carretera Federal Cuernavaca-Cuautla, No. 8534, Col. Progreso, CP 62550 Jiutepec, Morelos, Mexico^f Pakistan Academy of Sciences, Islamabad, Pakistan

ARTICLE INFO

Article history:

Received 26 August 2021

Revised 18 January 2022

Accepted 25 May 2022

Available online 30 May 2022

Keywords:

Oxalis pes-caprae

Phytochemicals

Antioxidant

Antibacterial

Cytotoxicity

FTIR

Molecular docking

SARS CoV-2 Mpro

ABSTRACT

Phytochemicals are directly involved in therapeutic treatment or precursors to synthesize useful drugs. The current study was aimed to evaluate the phytochemicals and their biopotentials using methanolic and n-hexane extracts of various parts of *Oxalis pes-caprae*. For the phytochemical analysis, standard procedures were used, whereas Aluminum Chloride reagent and Follin-ciocalteau reagent methods were used to determine total flavonoid and phenolic contents. Radical scavenging DPPH, phosphomolybdenum reduction, and reducing power assays were used to assess antioxidative potentials. Antibacterial potential was determined by applying disc diffusion method while cytotoxicity was determined employing brine shrimp assay. FT-IR (Fourier-transform infrared) analysis was utilized to gather spectral information, while molecular docking tools were employed to look at how *O. pes-caprae* plant-based ligands interact with the target protein COVID-19 3CLPro (PDB:6LU7). Phenols, flavonoids, alkaloids and saponins were tested positive in preliminary phytochemical studies. TPC and TFC in different extracts ranging from (38.55 ± 1.72) to (65.68 ± 0.88) mg/g GAE/g and (24.75 ± 1.80) to (14.83 ± 0.92) mg/g QUE/g were used respectively. IC₅₀ value (24.75 ± 0.76 g/mL) by OXFH, total antioxidant capacity (55.89 ± 1.75) mg/g by OXLM, reducing potential (34.98 ± 1.089) mg/g by OXSM, maximum zone of inhibition against *B. subtilis* (24 ± 0.65 mm) by OXLM and maximum cytotoxicity 96% with LD₅₀ 19.66 (μg/mL) by OXSM were the best calculated values among all extracts. Using molecular docking, it was found that Caeruleanone A, 2',4'-Dihydroxy-2''-(1-hydroxy-1-methylethyl) dihydrofuro [2,3-h] flavanone and Vadimezan demonstrated best affinity with the investigated SARS CoV-2 Mpro protein. This work provide justification about this plant as a source of effective phytochemicals and their potential against microbes could lead to development of biosafe drugs for the welfare of human being. In future, different *in vitro* and *in vivo* biological studies can be performed to further investigate its biomedical potentials.

© 2022 The Author(s). Published by Elsevier B.V. on behalf of King Saud University. This is an open access article under the CC BY-NC-ND license (<http://creativecommons.org/licenses/by-nc-nd/4.0/>).

* Corresponding authors.

E-mail addresses: javed89qau@gmail.com (J. Iqbal), amaro.estrada@gmail.com (I. Amaro-Estrada), tmahmood@qau.edu.pk (T. Mahmood).

Peer review under responsibility of King Saud University.



Production and hosting by Elsevier

1. Introduction

A temperate and Mediterranean invasive weed plant, *Oxalis pes-caprae* (family Oxalidaceae) (DellaGreca et al., 2009) also known as Bermuda buttercup is a highly clonal, polyploid medicinal plant (Barrett, 2015). In cultivated areas it tends to do best on heavy, well-drained soil (DellaGreca et al., 2008). Oxalic acid is responsible for sour taste of this plant in large herbivores and can cause nervous system paralysis, if taken in excessive amount (Herbert and Dittmer, 2017). For centuries, Oxalis roots have been used in folk medicines for their diuretic and leaves for antihypertensive

<https://doi.org/10.1016/j.jksus.2022.102136>

1018-3647/© 2022 The Author(s). Published by Elsevier B.V. on behalf of King Saud University.

This is an open access article under the CC BY-NC-ND license (<http://creativecommons.org/licenses/by-nc-nd/4.0/>).

properties (Gaspar et al., 2018). Oxalis species have recently been evaluated for their nutritional values. *Oxalis acetosella* is a rich source of B-carotenes, tocopherols, ascorbic acid, and xanthophylls, as well as flavonoids, especially rutin (Šircelj et al., 2010). The aerial parts of *O. pes-caprae* contained phenols, ester, phenyl cinnamate derivatives, aromatic compounds, cinnamic acid ester, two dihydrocinnamic acid esters, cinnamic and dihydrocinnamic acids, phenols and coumarins. Two compounds, 2-methoxyphenyl 3-phenyl-propanoate, and 2-hydroxyethyl 3-phenylpropanoate are reported first time as natural products from *O. pes-caprae* (DellaGreca et al., 2008; DellaGreca et al., 2009; DellaGreca et al., 2010). The conjugates of cinnamic acid with primaquine, were observed effective against human coronavirus (Pavić et al., 2016).

The sequence type of COVID-19 has a nucleotide sequence similarity of 82% with human SARS-CoV (severe acute respiratory syndrome) sequence (Chan et al., 2020; Lee and Hsueh, 2020; Xu et al., 2020). Prof. Zihé Rao and his investigation squad recently succeeded in expressing the COVID-19 3C-Like Proteinase. In a short time, the crystal structure of COVID-19 3CLpro (PDB: 6LU7) was described and determined (Liu et al., 2020). The chymotrypsin-like protease is well-known for its importance in the virus's life cycle, and the protease is stable within -coronaviruses. As a result, the COVID-19 3CLpro may be a candidate for new anti-COVID-19 drugs.

In this regard, we have conducted research using *Oxalis pes-caprae* as low-cost, renewable bioactive natural product sources. In the present study, *in vitro* antibacterial and, antioxidant activity of *O. pes-caprae*'s different extracts carried out. To explore the potential of natural compounds from *Oxalis pes-caprae* by *in silico* molecular docking studies that target the main protease (Mpro) of SARS CoV-2 to discover lead compound for clinical use.

2. Materials and methods

2.1. Plant collection and extract preparation

Fresh plants i.e., *Oxalis pes-caprae* L. at flowering stage (leaves, stem, and flowers) were collected from Bhakkar 31°-36' 29.554166" North latitude and 71°-5' 7.85588" East longitude at a height of 531 ft. above sea level during the months of March and April 2018 and was identified from Herbarium of Quaid-I-Azam University, Islamabad, Pakistan. Plants were dried under shade, powered and then kept in contact with methanol and n-hexane in a concentration of 30 g/300 mL for one week. After filtration, supernatants were collected, and the solvents were evaporated to make the crude extracts and maintained at 4 °C for further studies.

2.2. Phytochemical analysis

The extracts of all plant parts underwent phytochemical analysis to check the presence or absence of phenols by using Ferric chloride test, alkaloids by Mayer's test, flavonoids by Ammonium test and saponins by Froth test with little modifications (Uma and Sekar, 2014; Ahmed et al., 2017).

2.3. Total phenolic and flavonoid contents

To check total phenolic contents, Folin-Ciocalteu reagent was used. Calibration curve was generated by mixing 90 µL Folin-Ciocalteu reagent and 90 µL NaCO₃ solution with gallic acid. Similarly, each plant extract of 20 µL was mixed with reagent and absorbance was measured, as stated by Krishnaiah et al. (2015) with few modifications. Total flavonoid content was measured by applying method of Aluminium Chloride Colorimetric and the total

flavonoid contents were articulated as quercetin (mg) equivalents per gram of sample (Mak et al., 2013).

2.4. In vitro antioxidant activities

2.4.1. Free radical scavenging activity (DPPH Assay)

Antioxidative assays were performed as stated by Iqbal et al. (2019a,b) with some modifications. The DPPH (1,1-Diphenyl-2-picryl hydrazyl) assay was used to detect free radical scavenging activity, in which various concentrations of methanolic and n-hexane extracts have been pipetted out in test tubes. Freshly prepared 190 µL DPPH solution was added to each tube containing 10 µL of plant samples to make final volume of 200 µL. Resulted mixtures were left for incubation in dark for half an hour at room temperature and absorbance was checked at 517 nm. Ascorbic acid used as control. The percentage inhibition was determined by following formula.

$$\text{Percent scavenging of sample} = \frac{\text{Abs. of control} - \text{Abs. of sample}}{\text{Abs of control}} \times 100$$

2.4.2. Total antioxidant capacity (phosphomolybdenum reduction assay)

To determine total antioxidant capacity (TAC), each plant sample of 100 µL from stock solution mixed with 900 µL of reagent (The reagent used was prepared by mixing sodium phosphate 28 mM, ammonium molybdate 4 mM, sulfuric acid 0.6 M), followed by incubation for 90 min at 95 °C. After cooling at room temperature, the absorbance of each testing sample was measured at 630 nm in spectrophotometer. Ascorbic acid under same conditions served as standard.

2.4.3. Reducing power assay

For this assay, 100 µL each plant sample mixed with 250 µL (1%) potassium ferricyanide solution and 200 µL phosphate buffer (0.2 M) incubated for 20 mins at 50 °C in water bath. Then, 200 µL trichloroacetic acid added and centrifugation done at 3000 rpm for 10 min. After centrifugation, 150 µL supernatant picked and mixed with 50 µL (0.1%) ferric chloride and absorbance of resultant mixture was measured at 630 nm by a microplate reader. Gallic acid served as positive control and reduction potential was recorded as gallic acid equals to mg/g of extract.

2.5. Antibacterial potential (disc diffusion method)

This assay was performed as narrated by Alabri et al. (2014), with little modifications. In this assay, 100 µL inoculum of 24 h grown five bacterial strain *Escherichia coli* (ATCC 33456), *Pseudomonas aeruginosa* (ATCC 90271), *Bacillus subtilis* (ATCC 19659), *Staphylococcus aureus* (ATCC 6538) and *Klebsiella pneumonia* (ATCC 1705) was spread on the media pates with sterile cotton swabs. Paper disc of 6 mm diameters were soaked with 25 µL of the stock solution of several concentrations (100, 60, 50, 30, 20, and 10 µg/mL) of each extract loaded on plates having bacterial inoculum. After incubation for 24 h at 37 °C, their MIC values were measured. Oxytetracycline used as standard.

2.6. Brine shrimp cytotoxicity assay

The brine shrimp's lethality potential was assessed at various extract concentrations. Ocean Star (*Artemia salina*) eggs were hatched for 24 h in artificial sea water (3.8% sea salt augmented with 6 mg/ml yeast at pH 7). Plant extracts in various concentrations (1000, 500, 250, 62.5, and 31.25 µL) were poured into the

vials and the final volume was raised to 5 mL using an artificial sea salt solution. After 24 h, 10 brine shrimps were placed into each vial and incubated for 24 h at 32°Celsius, with living shrimps were counted in each vial. Finally, *Artemia salina* LC₅₀ values and percent mortality were determined (Supraja et al., 2018).

2.7. Fourier transform infrared spectroscopy analysis (FTIR)

To analyze the spectral information of plant samples, FTIR spectra in range of 400–4000 nm were recorded with a FTIR spectrophotometer.

2.8. Molecular docking data preparation

Twenty-four phytocompounds that are documented in *O. pes-caprae* were selected as ligands. The 2D molecular structures were retrieved from chemical database PubChem (Table 1). The

retrieved files were converted to PDB file format by using PyMOL software. The RCSB PDB (protein data bank) database was used to obtain the crystal structure of the protein COVID-19 3CLpro (PDB:6LU7). Three-dimensional (3D) structure of selected target protein is presented in Fig. 1. The files were saved as Target.pdb. Using AutoDock Vina tool (Trott and Olson, 2010), polar hydrogen atoms and Kollman partial charges were added to the 3D structures. The macromolecule file was written as. PDBQT file format for further analysis.

2.8.1. Molecular docking analysis

Docking calculations were performed using AutoDock Vina software. Ligands were docked into the target structures. For protein binding pocket the amino acids in the receptor's active site were identified, as stated in the protein analysis (Liu et al., 2020). In this study, the grid size was set to 60 × 60 × 60 points with 0.5 Å spacing centered on Mpro (6LU7). To study protein–ligand interactions,

Table 1

List of Chemical compounds (Ligands) applied in current study.

| S. No. | Chemical Compound | Formula | m/z | Compound CID | Reference |
|--------|-----------------------------------------------------------------------------|------------------------------------------------|--------------|--------------|-------------------------|
| 01 | Caeruleanone A | C ₂₈ H ₃₀ O ₇ | 478.5 g/mol | 102231361 | DellaGreca et al., 2010 |
| 02 | Loliolide | C ₁₁ H ₁₆ O ₃ | 196.24 g/mol | 100332 | – |
| 03 | Imperatorin | C ₁₆ H ₁₄ O ₄ | 270.28 g/mol | 10212 | DellaGreca et al., 2009 |
| 04 | Pterostilbene | C ₁₆ H ₁₆ O ₃ | 256.30 g/mol | 5281727 | – |
| 05 | Butylparaben | C ₁₁ H ₁₄ O ₃ | 194.23 g/mol | 7184 | – |
| 06 | Calycosin | C ₁₆ H ₁₂ O ₅ | 284.26 g/mol | 5280448 | – |
| 07 | Pelubiprofen | C ₁₆ H ₁₈ O ₃ | 258.31 g/mol | 5282203 | – |
| 08 | p-coumaric acid | C ₉ H ₈ O ₃ | 164.16 g/mol | 637542 | – |
| 09 | 3-Phenylpropionic acid | C ₉ H ₁₀ O ₂ | 150.17 g/mol | 107 | – |
| 10 | cis-p-Coumaric acid | C ₉ H ₈ O ₃ | 164.16 g/mol | 1549106 | – |
| 11 | Cinnamic acid | C ₉ H ₈ O ₂ | 148.16 g/mol | 444539 | – |
| 12 | 3-methoxyphenol | C ₇ H ₈ O ₂ | 124.14 g/mol | 9007 | – |
| 13 | 2- methoxyphenol | C ₉ H ₁₀ O ₂ | 167.2 g/mol | 1669 | – |
| 14 | 4-hydroxybenzoic acid | C ₇ H ₆ O ₃ | 138.12 g/mol | 135 | – |
| 15 | 2,6-Ditert-butyl-4-(1-hydroxyethyl) phenol | C ₁₆ H ₂₆ O ₂ | 250.38 g/mol | 12576677 | – |
| 16 | 3-(1-hydroxyethyl) phenol | C ₈ H ₁₀ O ₂ | 138.16 g/mol | 13542886 | – |
| 17 | Tangeretin | C ₂₀ H ₂₀ O ₇ | 372.4 g/mol | 68077 | – |
| 18 | Nobiletin | C ₂₁ H ₂₂ O ₈ | 402.4 g/mol | 72344 | – |
| 19 | Demethylnobiletin | C ₂₀ H ₂₀ O ₈ | 388.4 g/mol | 358832 | – |
| 20 | Vadimezan | C ₁₇ H ₁₄ O ₄ | 282.29 | 123964 | DellaGreca et al., 2008 |
| 21 | Zapotin | C ₁₉ H ₁₈ O ₆ | 342.3 | 629965 | – |
| 22 | 2',4'-Dihydroxy-2''-(1-hydroxy-1-methylethyl) dihydrofuro [2,3-h] flavanone | C ₂₀ H ₂₀ O ₆ | 356.4 | 10291777 | – |
| 23 | 2'-Hydroxy-3,4,4',6'-tetramethoxychalcone | C ₁₉ H ₂₀ O ₆ | 344.4 | 5373259 | – |
| 24 | Matairesinol | C ₂₀ H ₂₂ O ₆ | 358.4 | 119,205 | – |

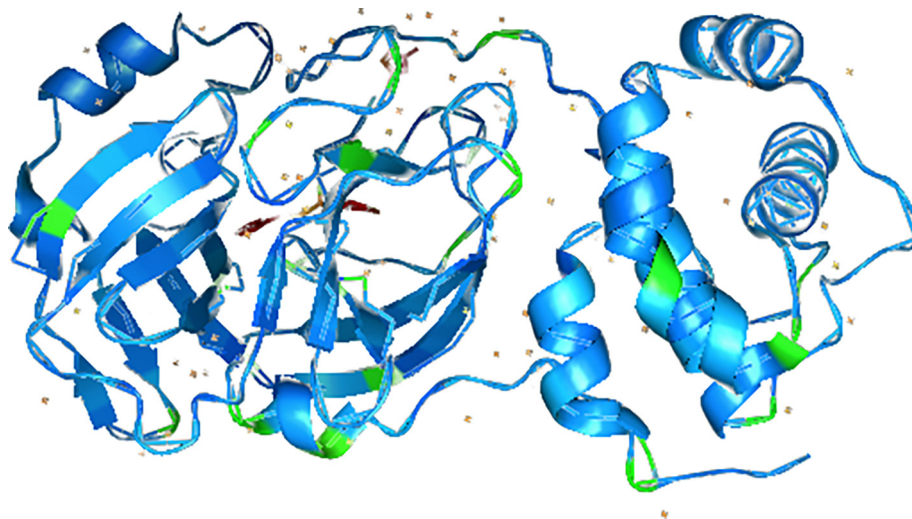


Fig. 1. Three-dimensional structure of 6LU7 main protease (Mpro): [PDB accession ID: 002214U].

Table 2
Total flavonoid and phenolic contents.

| Plant extracts | Total flavonoid contents (quercetin mg/g) | Total phenolic contents (gallic acid mg/g) |
|----------------|-------------------------------------------|--------------------------------------------|
| OXFM | 24.75 ± 1.80 | 65.68 ± 0.88 |
| OXFH | 22.93 ± 1.82 | 38.55 ± 1.72 |
| OXS | 16.98 ± 1.31 | 53.94 ± 1.48 |
| OXSH | 14.83 ± 0.92 | 41.01 ± 1.19 |
| OXML | 23.35 ± 1.35 | 57.04 ± 1.48 |
| OXLH | 18.95 ± 0.51 | 61.41 ± 1.55 |

Abbreviations: OXFM = *O. pes-caprae* flower methanol; OXFH = *O. pes-caprae* flower n-hexane; OXS = *O. pes-caprae* stem methanol; OXSH = *O. pes-caprae* stem n-hexane; OXML = *O. pes-caprae* leave methanol; OXLH = *O. pes-caprae* leave n-hexane.

Table 3
Brine shrimp cytotoxicity and DPPH scavenging assay.

| Plant samples | Brine shrimp lethality (µg/mL) | | DPPH scavenging activity |
|---------------|----------------------------------|------------------|--------------------------|
| | Percentage mortality 250 (µg/mL) | LD ₅₀ | IC ₅₀ (µg/mL) |
| OXFM | 82.1 ± 2.42 | 26.46 ± 1.64 | 36.36 ± 0.56 |
| OXFH | 61.90 ± 2.76 | 51.06 ± 2.11 | 24.57 ± 0.76 |
| OXS | 96.66 ± 1.89 | 19.66 ± 1.98 | 57.1 ± 0.65 |
| OXSH | 76.28 ± 1.60 | 48.78 ± 2.06 | 66.8 ± 0.67 |
| OXML | 53.29 ± 1.73 | 78.56 ± 1.57 | 46.3 ± 0.76 |
| OXLH | 44.31 ± 2.11 | 102.87 ± 1.90 | 56.2 ± 0.87 |
| Ascorbic acid | – | – | 23.74 ± 0.01 |

Abbreviations: OXFM = *O. pes-caprae* flower methanol; OXFH = *O. pes-caprae* flower n-hexane; OXS = *O. pes-caprae* stem methanol; OXSH = *O. pes-caprae* stem n-hexane; OXML = *O. pes-caprae* leave methanol; OXLH = *O. pes-caprae* leave n-hexane.

the Lamarckian Genetic Algorithm (LGA) was used. For other parameters, default setting was applied. The grid and docking parameter files were created with AutoDock tools. Configuration text file was generated to coordinate the specific set parameters for performing molecular docking of selected dataset, after running the script file you will have the result of top ten models with the best confirmations of docked complex, the topmost result with the low energy model selected as the best because it is based on the best bound ligand pose in the protein binding pocket. For each ligand, twenty-four independent runs were completed.

2.8.2. Protein–ligand complex analysis

The software LigPlot was used to analyze and visualize protein–ligand interaction. The software was also used to analyze and characterize the polar and hydrophobic interactions between the ligand and the target, in a docked protein–ligand complex. The illustrations of these kind of instructions were created.

3. Result

3.1. Preliminary phytochemical test

The qualitative screening of all plant parts demonstrated the presence of biologically active compounds such as alkaloids, flavonoids, phenols, and saponins. All parts of plant, especially leaves contain abundance of phytochemicals (Abbasi et al., 2020b). The phytochemicals are known to have medicinal importance being chemotherapeutic and chemo preventive sources (Abbasi et al., 2018; Iqbal et al., 2019a,b), as alkaloids derived from medicinal plants have biological properties like anti-cancer (Gupta et al., 2015; Abbasi et al., 2019), anti-larval (Qi et al., 2010), antimicrobial (Greger, 2017; Adamski et al., 2020), and insecticidal potential (Greger, 2019). Flavonoids are extensively used in medicine as anti-cancer (Zhao et al., 2019), antioxidant, antimalarial, antitumor, anti-proliferative, neuroprotective (Patel et al., 2018), and antiangiogenic

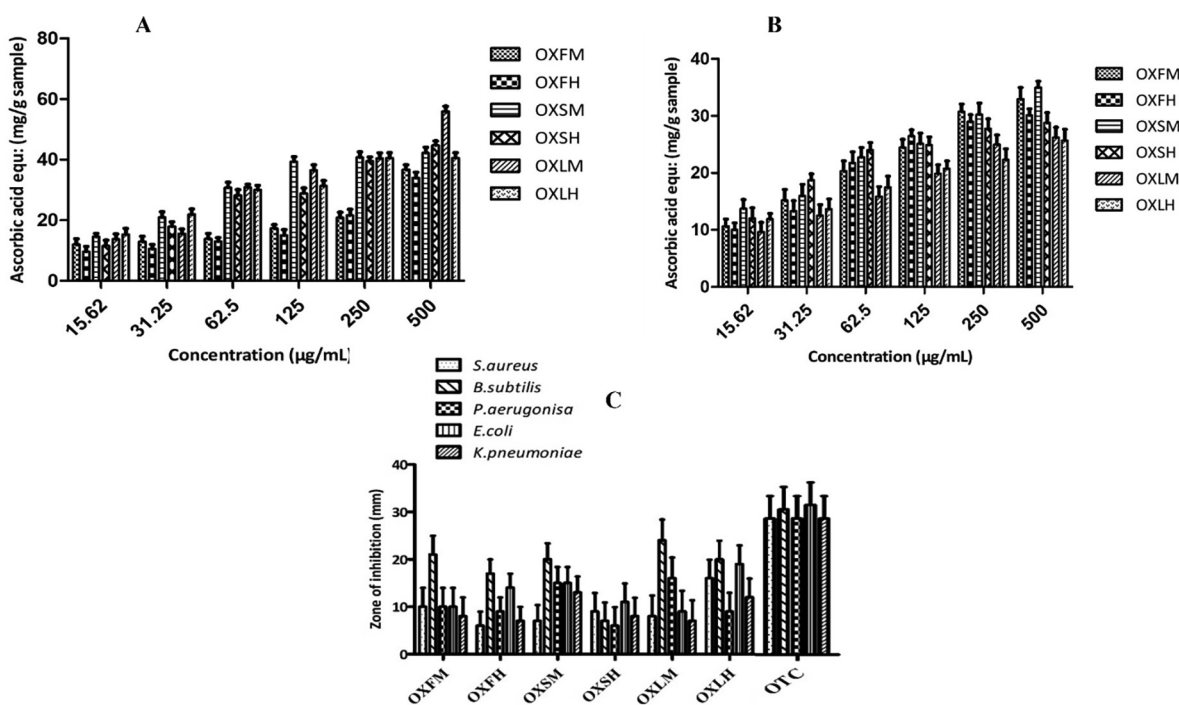


Fig. 2. (A) Total antioxidant capacity (B) total reducing power and (C) antibacterial potential exhibited by different extracts of *O. pes-caprae*. Through triplicate analysis (means ± SD) were obtained. Abbreviations: OXFM = *O. pes-caprae* flower methanol; OXFH = *O. pes-caprae* flower n-hexane; OXS = *O. pes-caprae* stem methanol; OXSH = *O. pes-caprae* stem n-hexane; OXML = *O. pes-caprae* leave methanol; OXLH = *O. pes-caprae* leave n-hexane; OTC = Oxytetracycline.

agents (Camero et al., 2018). Similarly, phenols and saponins have defensive properties for various ailment (Shoker, 2020) and anti-diabetic potential (Uzayisenga et al., 2014) respectively. These phytochemical substances found in the plants could be responsible for *O. pes-caprae* biological potential, as well as its traditional medicinal uses.

3.2. Total phenolic and flavonoid contents

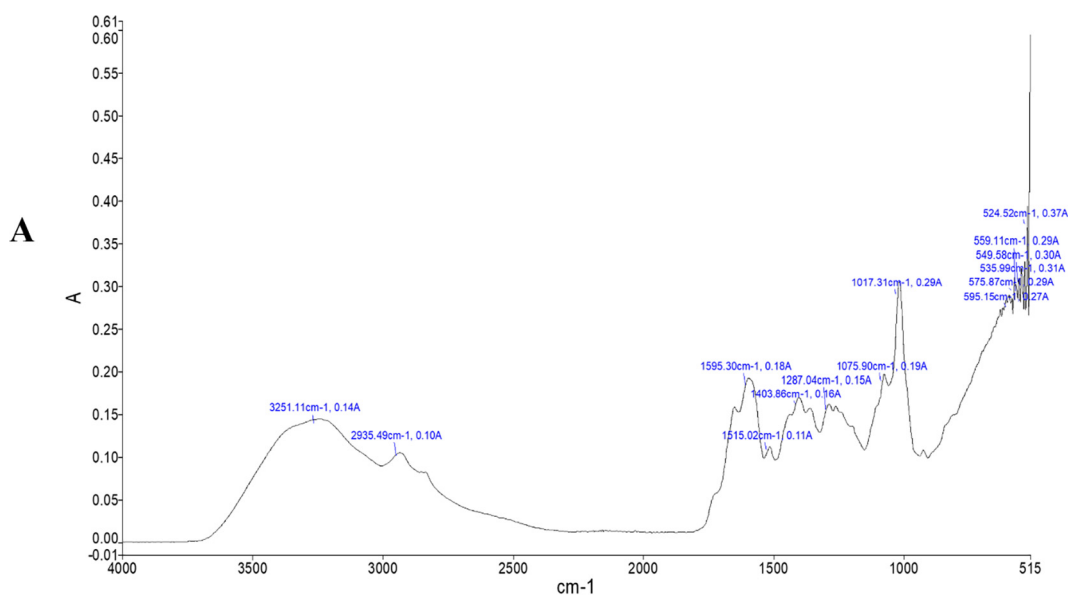
Any plant's pharmacological potential is determined by secondary metabolites and phenolic chemicals that are involved in the maintenance of detoxification (Zahra et al., 2021). The presence of total phenolic and total flavonoid contents in the plant extracts are presented in Table 2. Güçlütürk et al. (2012) evaluated methanolic extracts of *O. pes-caprae* (arial parts) with total phenolic contents as (4.16 ± 0.32) mg/g. In current studies, TPC and TFC varied greatly, and ranged from (38.55 ± 1.72) to (65.68 ± 0.88) mg/g GAE/g and (24.75 ± 1.80) to (14.83 ± 0.92) mg/g QUE/g, of different extracts respectively.

3.3. In vitro antioxidant activities

Plant's antioxidant and radical-scavenging abilities are linked to their therapeutic qualities. The IC₅₀ value which shows the

quantity of antioxidant required to reduce radical concentration by 50%, is negatively associated to antioxidant capacity (Basuny et al., 2012). Three distinct assays were used to access antioxidant activity in this investigation, namely DPPH, TAC and, reducing power assay. By DPPH free radical scavenging assay, best calculated IC₅₀ value $(24.57 \pm 0.76 \mu\text{g/mL})$ by OXFH, while lowest potential exhibited by n-hexane extract of stem was $(66.8 \pm 0.67 \mu\text{g/mL})$. Depicted IC₅₀ values by various parts of *O. pes-caprae* were as followed OXFH (24.57 ± 0.76) , OXFM (36.36 ± 0.56) , OXLM (46.3 ± 0.76) , OXLH (56.2 ± 0.87) , OXSM (57.1 ± 0.65) , and OXSH $(66.8 \pm 0.67) \mu\text{g/mL}$ presented in Table 3. GraphPad Prism Software was used to create a percent DPPH scavenging activity by IC₅₀ values.

The phosphomolybdate assay was applied to evaluate the total antioxidant capacity (TAC). This assay is used to access a chemical's ability to scavenge ROS (Abbasi et al., 2020a). The assay is because when a reducing agent (antioxidant) is present, molybdenum (VI) is reduced to molybdenum(V), generating a green color phosphomolybdate(V) complex, that maybe spectrophotometrically assessed (Jan et al., 2013). Total antioxidant capacity is a significant tool for inspecting the correlation of antioxidants and pathologies incited by the oxidative stresses (Pisoschi and Negulescu, 2011). Total antioxidant capacity of selected plants was expressed as ascorbic acid equivalent mg/g of each extract shown in Fig. 2(A).



| Absorbance (cm ⁻¹) | Bond | Functional group |
|--------------------------------|------------------------|--------------------------------------------|
| 3251.11 | O–H stretch | carboxylic acids |
| 2935.49 | C–H stretch | Aromatics |
| 1595.30 | C–C stretch (in–ring) | Aromatics |
| 1515.02 | N–O asymmetric stretch | nitro compounds |
| 1403.88 | C–C stretch (in–ring) | Aromatics |
| 1287.04 | C–N stretch | aromatic amines |
| 1075.90 | C–O stretch | alcohols, carboxylic acids, esters, ethers |
| 1017.31 | C–O stretch | alcohols, carboxylic acids, esters, ethers |
| 595.15 | C–Br stretch | alkyl halides |

Fig. 3. (A; B) FTIR analysis displays the functional groups and frequency range of inorganic and organic compounds in *O. pes-caprae* flower.

Highest value of TAC was (55.89 ± 1.758 mg/g) observed by OXLM, lowest value was (33.98 ± 1.874 mg/g) by OXFH.

The principle of reducing power assay work as, the reducers i.e., antioxidants cause the reduction of Fe^{3+} /ferricyanide complex to ferrous form. As a result, the Perl's Prussian Blue production can be utilized to observe Fe^{2+} content (Ferreira et al., 2007). Reducing potential of plants is calculated by total reducing power assessment as shown in Fig. 2(B) with maximum value (34.98 ± 1.089 mg/g) by OXSM.

3.4. Screening of crude extracts for antibacterial activity (Disc diffusion assay)

Plants are a potent source of phytochemicals which play an incredible role against microorganisms. To assess the antibacterial potential of selected plants disc diffusion method was applied. Plant extracts were tested for antibacterial activity against gram +ve (*B. subtilis*, *S. aureus*) and gram negative (*E. coli*, *K. pneumoniae*, and *P. aeruginosa*) bacteria. Antibacterial potential as evaluated by zone of inhibition showed significant variation. After 24 h of incubation, the maximum zone of inhibition by extracts of *O. pes-caprae* leave for both methanol and n-hexane were observed against *B. subtilis* as (24 ± 0.65 mm) and (20 ± 0.34 mm) respectively. For *S. aureus*, *P. aeruginosa*, *E. coli* and *K. pneumoniae* maximum inhibition were (16 ± 0.45) by OXLH, (19 ± 0.34) by OXLH and (13 ± 0.23) mm by OXSM respectively. Fig. 2 (C) graphically representing zone of inhibition of *O. pes-caprae* extracts.

3.5. Brine shrimp cytotoxicity assay (BSCA)

The appropriate assay for determination of cytotoxicity of plants extracts and their assorted compounds is, BSCA (Olowa and Nuñez, 2013). The findings revealed a concentration-dependent response, with an increase in concentration of extract, leading to an increase in brine shrimps' mortality, whereas a decrease in plant extract concentration leads to a decrease in mortality. In *O. pes-caprae* extracts, lethality was observed, indicating the presence of potent cytotoxicity. Among all extracts of *O. pes-caprae*, OXSM and OXFM exhibited high percentage of mortality of *Artemia salina* of 96 and 82%, with LD_{50} 19.66 and 26.46 ($\mu\text{g}/\text{mL}$) respectively (Table 3).

3.6. Fourier transform infrared spectroscopy (FTIR)

Fourier transform infrared spectroscopy applied to identify functional groups and type of chemical bonds that exist in phytochemicals. The main component of chemical bonding is light absorbed wavelength, which may be seen through a spectrum interpretation. By analyzing the absorption infrared spectrum, compound chemical bonds can be determined (Ahmad et al., 2016). In the present study functional groups were examined using FTIR spectroscopy based on their absorbance (Figs. 3 and 4). The peaks obtained from the analysis were decoded and the functional groups were determined. The functional groups present in the plant sample refers to specific class of compounds (Figs. 3; 4).

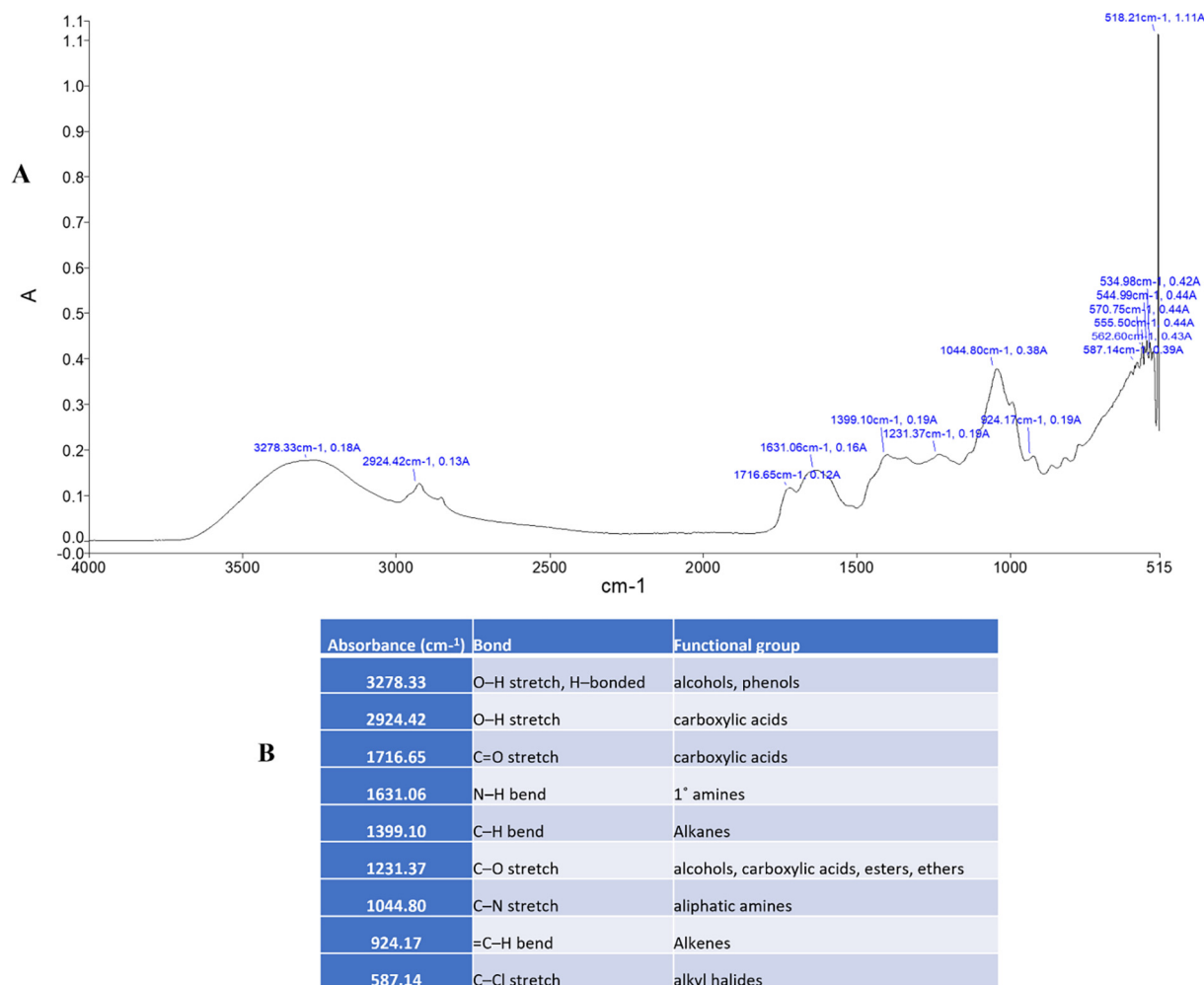
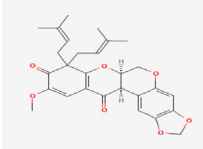
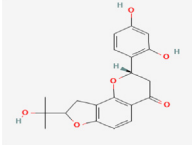
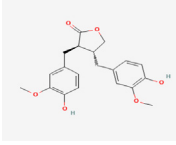
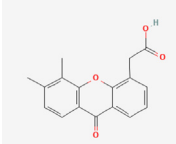
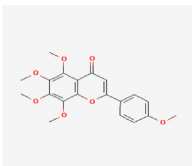
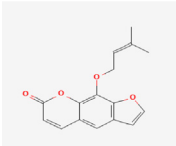
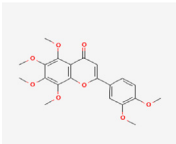
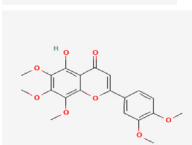
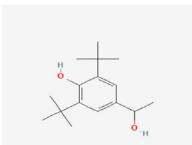
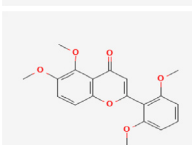


Fig. 4. (A; B) FTIR analysis displays the functional groups and frequency range of inorganic and organic compounds in *O. pes-caprae* stem.

Table 4

Two-dimensional structures and the binding strength of investigated ligands with the SARS CoV-2 protein.

| S. No. | Chemical Compound | Chemical structure | Binding affinity (kcal/mol) |
|--------|-----------------------------------------------------------------------------|--------------------------------------------------------------------------------------|-----------------------------|
| 01 | Caeruleanone A |  | -11.1 |
| 02 | 2',4'-Dihydroxy-2''-(1-hydroxy-1-methylethyl) dihydrofuro [2,3-h] flavanone |  | -10.5 |
| 03 | Matairesinol |  | -10.3 |
| 04 | Vadimezan |  | -9.6 |
| 05 | Tangeretin |  | -9.3 |
| 06 | Imperatorin |  | -9.2 |
| 07 | Nobiletin |  | -9.2 |
| 08 | Demethylnobiletin |  | -9.2 |
| 09 | 2,6-Ditert-butyl-4-(1-hydroxyethyl) phenol |  | -9.1 |
| 10 | Zapotin |  | -9.0 |

(continued on next page)

Table 4 (continued)

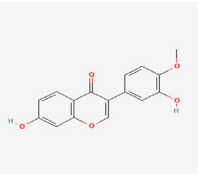
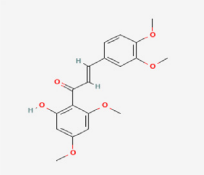
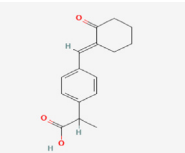
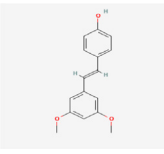
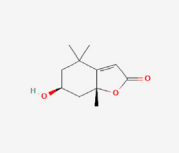
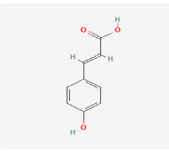
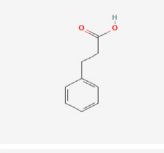
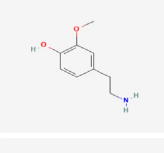
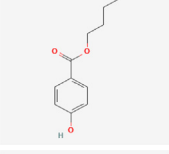
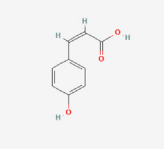
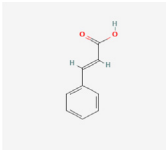
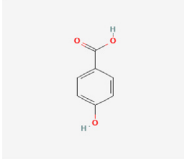
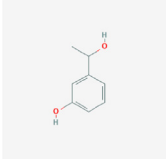
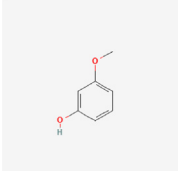
| S. No. | Chemical Compound | Chemical structure | Binding affinity (kcal/mol) |
|--------|-------------------------------------------|--------------------------------------------------------------------------------------|-----------------------------|
| 11 | Calycosin |  | -8.7 |
| 12 | 2'-Hydroxy-3,4,4',6'-tetramethoxychalcone |  | -8.6 |
| 13 | Pelubiprofen |  | -8.5 |
| 14 | Pterostilbene |  | -7.7 |
| 15 | Loliolide |  | -7.2 |
| 16 | p-coumaric acid |  | -6.7 |
| 17 | 3-Phenylpropionic acid |  | -6.6 |
| 18 | 2-methoxyphenol |  | -6.5 |
| 19 | Butylparaben |  | -6.5 |
| 20 | cis-p-Coumaric acid |  | -6.5 |

Table 4 (continued)

| S. No. | Chemical Compound | Chemical structure | Binding affinity (kcal/mol) |
|--------|---------------------------|------------------------------------------------------------------------------------|-----------------------------|
| 21 | Cinnamic acid |  | -6.1 |
| 22 | 4-hydroxybenzoic acid |  | -6.1 |
| 23 | 3-(1-hydroxyethyl) phenol |  | -5.7 |
| 24 | 3-methoxyphenol |  | -5.0 |

3.7. Molecular docking results

After docking process, the ligands were classified according to their protein-ligands binding energies. The results were analyzed based on the interactions between SARS Covid-2 protein and the compounds as well as the binding energies of the complexes. Target protein and chemical compounds are the requirements to start the molecular docking procedure. Previously reported 24 compounds from *O. pes-caprae* were used as datasets for molecular docking studies. The two-dimensional structures of selected 24 compounds were drawn very carefully by ChemDraw Ultra 12.0 software illustrated in Table 4. Three-dimensional structure of selected targeted protein; 6LU7 protein was recovered from protein data bank (accession ID 002214) with resolution 2.16 Å. These natural compounds were expected to have anti-viral potential, so it is validated by the application of computer-aided drug design procedures, such as the calculation of protein-ligand binding interaction behavior with 6LU7 protein target, which is one of the novel therapeutic agents to design potential drugs for COVID-19. Results for binding energy (kcal/mol) of selected phytochemical compounds with the COVID-19 3clpro/Mpro (PDB ID: 6LU7) using Auto Dock vina are summarized in Table 5. The ligands bind to the active site of the 6LU7 protein with significant binding energy in the same hydrophobic pocket as the Diclofenac regulation, according to docking studies. In the current study we find that Caeruleanone A, 2',4'-Dihydroxy-2''-(1-hydroxy-1-methylethyl) dihydrofuro [2,3-h] flavanone and Vadimezan demonstrated best affinity with the investigated SARS CoV-2 Mpro protein.

Summary of the molecular docking results of 14 potential hits are given in Table 5 also include docking parameters including binding energy and FF score alongside the amino acids (residues) contained in active site pockets of 6LU7. Caeruleanone A presented highest binding affinity -11.1 Kcal/mol as compared to other compounds and formed nine hydrophobic interactions with Thr111(A), Asn151(A), Phe294(A), Phe8(A), Asp153(A), Ile152(A), Arg105(A),

Ile106(A) and Gln107(A) residues and formed one hydrogen bond with Gln107(A) residue with length of 2.89 Å. 2',4'-Dihydroxy-2''-(1-hydroxy-1-methylethyl) dihydrofuro [2,3-h] flavanone formed four hydrophobic interactions with Ile152(A), Asn151(A), Gln110(A), Phe294(A) and Val104(A) residues and four hydrogen bonds with three different residues Ser158(A) (1), Asp153(A) (1) and Thr111(A) (2). The interactions resulted in very good binding energy of -10.5 Kcal/mol. Matairesinol formed seven hydrophobic interactions with Gln110(A), Ile106(A), Asn151(A), Val104(A), Asp153(A), Phe294(A) and Ile152(A) residues and only one hydrogen bond with Thr111(A) residue of Mpro target protein with bond distance of 3.17 Å. Although the interactions resulted in the binding energy of -10.3 Kcal/mol.

Likewise, Vadimezan also formed five hydrophobic interactions with Gln110(A), Thr292(A), Phe294(A), Asn151(A) and Ile106(A) residues and three hydrogen bonds with Thr111(A) residue with length of 3.14, 2.93 and 2.83 Å. These interactions resulted in binding energy of -9.6 Kcal/mol. Tangeretin presented very good binding affinity -9.3 kcal/mol during docking and formed seven hydrophobic interactions with Phe294(A), Asn151(A), Arg105(A), Val104(A), Ile106(A), Thr111(A) and Gln110(A) residues of targeted protein but no hydrogen bonding was observed. Imperatorin showed good binding energy -9.2 kcal/mol and formed hydrophobic interactions with Gln110(A), Gln107(A), Ile106(A), Asn151(A), Phe294(A) and Thr292(A) residues and two hydrogen bonds with Thr111(A). Nobiletin resulted in -9.2 kcal/mol binding energy during docking analysis. Nobiletin also illustrated hydrophobic interactions with Thr111(A), Asn151(A), Phe294(A), Gln110(A), Ile106(A), Arg105(A) and Val104(A) residues of 6LU7 target protein but no hydrogen bonding has been observed. Demethylnobiletin during molecular docking investigation presented good binding affinity (-9.2 kcal/mol). Formed six hydrophobic interactions with Phe294(A), Asn151(A), Ile106(A), Gln110(A), Arg105(A) Val104(A) residues and one hydrogen bond was also observed with Thr111(A) residue. 2,6-Ditert-butyl-4-(1-hydroxyethyl) phenol presented

Table 5

Interactions plots and interacting residues of fourteen potential hits with the SARS CoV-2 Mpro proteins are summarized with the number of hydrophobic interactions and the number of hydrogen bonds (where red spikes represent hydrophobic residues, green-colored residues represent hydrogen bonds).

| S. No. | Chemical Compound | Functional Residues Involved in Hydrophobic Interactions | Total Hydrogen Bonds with Distance | Interaction plots | Binding affinity (kcal/mol) |
|--------|-----------------------------------------------------------------------------|---------------------------------------------------------------------------------------------------------------------|--------------------------------------------------------------------------------------------------------------------------|-------------------|-----------------------------|
| 01 | Caeruleanone A | Thr111(A) Asn151(A) Phe294(A) Phe8(A) Asp153(A) Ile152(A) Arg105(A) Ile106(A) Gln107(A) | (1) Gln107(A) NE2- O3 = 2.89 Å | | -11.1 |
| 02 | 2',4'-Dihydroxy-2''-(1-hydroxy-1-methylethyl) dihydrofuro [2,3-h] flavanone | Ile152(A) Asn151(A) Gln110(A) Phe294(A) Val104(A) | (4) Ser158(A) OG-05 = 3.24 Å Asp153(A) OD2- O5 = 3.07 Å Thr111(A) OG1- O3 = 3.24 Å N-O3 = 3.20 Å | | -10.5 |
| 03 | Matairesinol | Gln110(A) Ile106(A) Asn151(A) Val104(A) Asp153(A) Phe294(A) Ile152(A) | (1) Thr111(A) OG1- O2 = 3.17 Å | | -10.3 |
| 04 | Vadimezan | Gln110(A) Thr292(A) Phe294(A) Asn151(A) Ile106(A) | (3) Thr111(A) O-03 = 3.14 Å N-O3 = 2.93 Å OG1- O3 = 2.83 Å | | -9.6 |

Table 5 (continued)

| S. No. | Chemical Compound | Functional Residues Involved in Hydrophobic Interactions | Total Hydrogen Bonds with Distance | Interaction plots | Binding affinity (kcal/mol) |
|--------|-------------------|-----------------------------------------------------------------------------------------|--------------------------------------------------|-------------------|-----------------------------|
| 05 | Tangeretin | Phe294(A) Asn151(A) Arg105(A) Val104(A) Ile106(A) Thr111(A) Gln110(A) | NO hydrogen bonding | | -9.3 |
| 06 | Imperatorin | Gln110(A) Gln107(A) Ile106(A) Asn151(A) Phe294(A) Thr292(A) | (2) Thr111(A) O4 = 2.75 Å N-O4 = 3.08 Å | | -9.2 |
| 07 | Nobiletin | Thr111(A) Asn151(A) Phe294(A) Gln110(A) Ile106(A) Arg105(A) Val104(A) | NO hydrogen bonding | | -9.2 |
| 08 | Demethylnobiletin | Phe294(A) Asn151(A) Ile106(A) Gln110(A) Arg105(A) Val104(A) | (1) Thr111(A) O-O5 = 3.19 Å | | -9.2 |

(continued on next page)

Table 5 (continued)

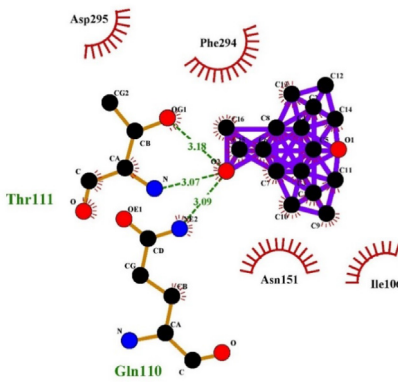
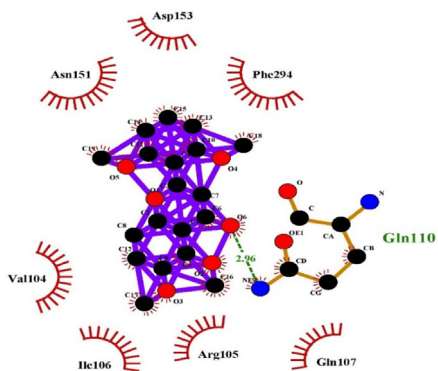
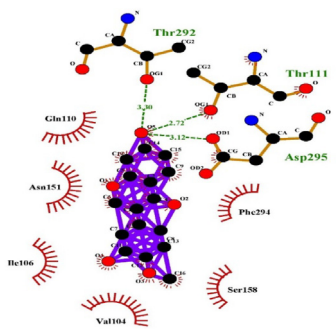
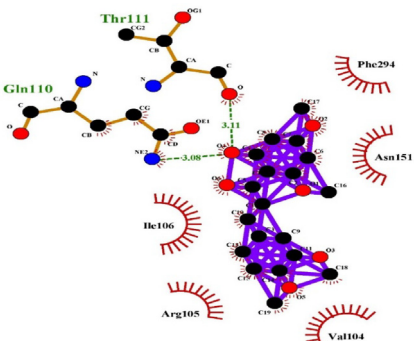
| S. No. | Chemical Compound | Functional Residues Involved in Hydrophobic Interactions | Total Hydrogen Bonds with Distance | Interaction plots | Binding affinity (kcal/mol) |
|--------|--------------------------------------------|---------------------------------------------------------------------------------------------|-----------------------------------------------------------------------------------------------------------------|--------------------------------------------------------------------------------------|-----------------------------|
| 09 | 2,6-Ditert-butyl-4-(1-hydroxyethyl) phenol | Asp295(A) Phe294(A) Asn151(A) Ile106(A) | (3) Thr111(A) OG1- O2 = 3.18 Å N-O2 = 3.07 Å Gln110(A) NE2- O2 = 3.09 Å |  | -9.1 |
| 10 | Zapotin | Gln107(A) Arg105(A) Ile106(A) Val104(A) Asn151(A) Asp153(A) Phe294(A) | (1) Gln110(A) NE2- O6 = 2.96 Å |  | -9.0 |
| 11 | Calycosin | Val104(A) Ile106(A) Phe294(A) Asn151(A) Ser158(A) Gln110(A) | (3) Asp295(A) OD1- O5 = 3.12 Å Thr292(A) OG1- O5 = 3.30 Å Thr111(A) OG1- O5 = 2.72 Å |  | -8.7 |
| 12 | 2'-Hydroxy-3,4,4',6'-tetramethoxychalcone | Ile106(A) Arg105(A) Val104(A) Asn151(A) Phe294(A) | (2) Thr111(A) O-O4 = 3.11 Å Gln110(A) NE2- O4 = 3.08 Å |  | -8.6 |

Table 5 (continued)

| S. No. | Chemical Compound | Functional Residues Involved in Hydrophobic Interactions | Total Hydrogen Bonds with Distance | Interaction plots | Binding affinity (kcal/mol) |
|--------|-------------------|------------------------------------------------------------------------------------|-----------------------------------------------------------------------------|-------------------|-----------------------------|
| 13 | Pelubiprofen | Gln110(A) Ile106(A) Val104(A) Asn151(A) Phe294(A) | (2) Thr111(A) OG1- O2 = 2.90 Å N-O3 = 3.19 Å (2) | | -8.5 |
| 14 | Pterostilbene | Gln110(A) Arg105(A) Ile106(A) Val104(A) Asn151(A) Phe294(A) | (2) Asp295(A) OD1- O3 = 3.15 Å Thr111(A) OG1- O3 = 2.92 Å | | -7.7 |

good network of hydrophobic interactions with Asp295(A), Phe294(A), Asn151(A) and Ile106(A) residues and three hydrogen bonds with Thr111(A) and Gln110(A) residues of Mpro target protein have been observed. The interactions resulted in the binding energy of -9.1 kcal/mol. Zapotin formed seven hydrophobic interactions with Gln107(A), Arg105(A), Ile106(A), Val104(A), Asn151(A), Asp153(A) and Phe294(A) residues and one hydrogen bond with Gln110(A) residue. Calycosin presented good binding energy (-8.7 kcal/mol) during docking analysis and showed hydrophobic interactions with Val104(A), Ile106(A), Phe294(A), Asn151(A), Ser158(A) and Gln110(A) and formed three hydrogen bonds with Asp295(A), Thr292(A) and Thr111(A) residues of 6LU7 target protein. 2'-Hydroxy-3,4,4',6'-tetramethoxychalcone, Pelubiprofen and Pterostilbene also presented very good network of hydrophobic interactions and hydrogen bonding interactions with binding affinity -8.6 , -8.5 and -7.7 respectively.

4. Conclusion

A viable and valuable alternative is plant derived bioactive molecules with pharmacological action. Many researchers have been enthralled by the prospect of discovering novel pharmacologically active phytoconstituents from plants, primarily to progress the treatment of various diseases. In this study we report that the methanolic and n-hexane extracts of various parts of *O. pes-caprae* contain different phytochemicals which have antioxidative and biological potential. These phytochemicals were further evaluated based on their binding energy against COVID-19 target protein. Knowing that many phytochemicals are already identified for their antiviral potential, we can refer to computational chemistry and bioinformatics resources to help in the study of dif-

ferent activities of medicinal plants. The 6LU7 Mpro has shown to be crucial and highly potent target for the inhibition of novel COVID-19. This study concludes 4 natural compounds (Caeruleanone A, 2',4'-Dihydroxy-2''-(1-hydroxy-1-methylethyl) dihydrofuro [2,3-h] flavanone, Matairesinol, Vadimezan) as a potential inhibitor of 6LU7 Mpro. Molecular docking analysis revealed that these molecules possess strong binding energy and interactions based on hydrogen bonding. These results can provide the outline for synthetic modification of bioactive compounds, de novo synthesis of structural motifs, and lead to additional phytochemical investigation. The information generated from this study may be utilized in future for development of more phytochemical-based therapeutics against COVID-19. In future, different *in vitro* and *in vivo* biological studies can be performed to further investigate its biomedical potentials.

5. Authors' contributions

FG and IK identified and collected plant. FG and JI, prepared/processed the plant extracts and performed experimental work. TM performed literature search and supervised the research project. Statistical analyses were conducted by RC, IAE, YABJ, RCB. BAA, SAA, AS and JI corrected and edited the manuscript written by FG. All the authors have read and finally approved the manuscript.

Declaration of Competing Interest

The authors declare that they have no known competing financial interests or personal relationships that could have appeared to influence the work reported in this paper.

Acknowledgement

The authors would like to extend their sincere appreciation to the Researchers Supporting Project Number (RSP2022R457), King Saud University, Riyadh, Saudi Arabia.

References

- Abbasi, B.A., Iqbal, J., Ahmad, R., Bibi, S., Mahmood, T., Kanwal, S., Bashir, S., Gul, F., Hameed, S., 2019. Potential phytochemicals in the prevention and treatment of esophagus cancer: A green therapeutic approach. *Pharmacol. Rep.* 71 (4), 644–652.
- Abbasi, B.A., Iqbal, J., Kiran, F., Ahmad, R., Kanwal, S., Munir, A., Uddin, S., Nasir, J.A., Chalgham, W., Mahmood, T., 2020a. Green formulation and chemical characterizations of *Rhannella gilgitica* aqueous leaves extract conjugated NiONPs and their multiple therapeutic properties. *J. Mol. Struct.* 1218, 128490.
- Abbasi, B.A., Iqbal, J., Mahmood, T., Khalil, A.T., Ali, B., Kanwal, S., Shah, S.A., Ahmad, R., 2018. Role of dietary phytochemicals in modulation of miRNA expression: Natural swords combating breast cancer. *Asian Pac. J. Trop. Med.* 11 (9), 501.
- Abbasi, B.A., Iqbal, J., Nasir, J.A., Zahra, S.A., Shahbaz, A., Uddin, S., Hameed, S., Gul, F., Kanwal, S., Mahmood, T., 2020b. Environmentally friendly green approach for the fabrication of silver oxide nanoparticles: Characterization and diverse biomedical applications. *Microsc. Res. Technol.* 83 (11), 1308–1320.
- Adamski, Z., Blythe, L.L., Milella, L., Bufo, S.A., 2020. Biological activities of alkaloids: from toxicology to pharmacology. *Toxins* 12 (4), 210.
- Ahmad, S., Abdel-Salam, N.M., Ullah, R. 2016. In vitro antimicrobial bioassays, DPPH radical scavenging activity, and FTIR spectroscopy analysis of *Heliotropium bacciferum*. *BioMed Res. Int.*, 2016.
- Ahmed, H., Irshad Khan, M.Z., Waseem, D., Nazli, A., Waleed Baig, M., 2017. Phytochemical analysis and antioxidant potential of *Ficus Benghalensis* L. *J. Bioresource Manage.* 4 (3), 3.
- Alabri, T.H.A., Al Musalami, A.H.S., Hossain, M.A., Weli, A.M., Al-Riyami, Q., 2014. Comparative study of phytochemical screening, antioxidant and antimicrobial capacities of fresh and dry leaves crude plant extracts of *Datura metel* L. *J. King Saud Univ.-Sci.* 26 (3), 237–243.
- Barrett, S. C. 2015. *Foundations of Invasion Genetics: the Baker and Stebbins Legacy*.
- Basuny, A.M., Arafat, S.M., El-Marzooq, M.A., 2012. Antioxidant and antiherpetic activities of anthocyanins from eggplant peels. *J. Pharma Res. Rev.* 2 (3), 50–57.
- Camero, C.M., Germanò, M.P., Rapisarda, A., D'Angelo, V., Amira, S., Benchikh, F., De Leo, M., 2018. Anti-angiogenic activity of iridoids from *Galium tunetanum*. *Rev. Bras. Farmacogn.* 28, 374–377.
- Chan, J.F.W., Kok, K.H., Zhu, Z., Chu, H., To, K.K.W., Yuan, S., Yuen, K.Y., 2020. Genomic characterization of the 2019 novel human-pathogenic coronavirus isolated from a patient with atypical pneumonia after visiting Wuhan. *Emerg. Microbes Infect.* 9 (1), 221–236.
- DellaGreca, M., Previtiera, L., Purcaro, R., Zarrelli, A., 2009. Phytochemical aromatic constituents of *Oxalis pes-caprae*. *Chem. Biodivers.* 6 (4), 459–465.
- DellaGreca, M., Previtiera, L., Zarrelli, A., 2010. A new aromatic component from *Oxalis pes-caprae*. *Nat. Prod. Res.* 24 (10), 958–961.
- DellaGreca, M., Purcaro, R., Previtiera, L., Zarrelli, A., 2008. Phenyl cinnamate derivatives from *Oxalis pes-caprae*. *Chem. Biodivers.* 5 (11), 2408–2414.
- Ferreira, I.C., Baptista, P., Vilas-Boas, M., Barros, L., 2007. Free-radical scavenging capacity and reducing power of wild edible mushrooms from northeast Portugal: Individual cap and stipe activity. *Food Chem.* 100 (4), 1511–1516.
- Gaspar, M.C., Fonseca, D.A., Antunes, M.J., Frigerio, C., Gomes, N.G., Vieira, M., Campos, M.G., 2018. Polyphenolic characterisation and bioactivity of an *Oxalis pes-caprae* L. leaf extract. *Nat. Prod. Res.* 32 (6), 732–738.
- Greger, H., 2017. Phytocarbazoles: Alkaloids with great structural diversity and pronounced biological activities. *Phytochem. Rev.* 16 (6), 1095–1153.
- Greger, H., 2019. Structural classification and biological activities of Stemona alkaloids. *Phytochem. Rev.* 18 (2), 463–493.
- Güçlütürk, I., Detsi, A., Weiss, E.K., Ioannou, E., Roussis, V., Kefalas, P., 2012. Evaluation of antioxidant activity and identification of major polyphenolics of the invasive weed *Oxalis pes-caprae*. *Phytochem. Anal.* 23 (6), 642–646.
- Gupta, A.P., Pandotra, P., Kushwaha, M., Khan, S., Sharma, R., Gupta, S., 2015. Alkaloids: a source of anticancer agents from nature. *Stud. Nat. Prod. Chem.* 46, 341–445.
- Herbert, E.W., Dittmer, K.E., 2017. Acute and chronic oxalate toxicity in Miniature Horses associated with soursob (*Oxalis pes-caprae*) ingestion. *Equine Vet. Educ.* 29 (10), 549–557.
- Iqbal, J., Abbasi, B.A., Ahmad, R., Batool, R., Mahmood, T., Ali, B., Khalil, A.T., Kanwal, S., Shah, S.A., Alam, M.M., Bashir, S., Badshah, H., Munir, A., 2019a. Potential phytochemicals in the fight against skin cancer: Current landscape and future perspectives. *Biomed. Pharmacother.* 109, 1381–1393.
- Iqbal, J., Abbasi, B.A., Mahmood, T., Kanwal, S., Ahmad, R., Ashraf, M., 2019b. Plant-extract mediated green approach for the synthesis of ZnONPs: Characterization and evaluation of cytotoxic, antimicrobial and antioxidant potentials. *J. Mol. Struct.* 1189, 315–327.
- Jan, S., Khan, M.R., Rashid, U., Bokhari, J., 2013. Assessment of antioxidant potential, total phenolics and flavonoids of different solvent fractions of *Monothea buxifolia* fruit. *Osong Public Health Res. Perspect.* 4 (5), 246–254.
- Krishnaiah, D., Bono, A., Sarbatly, R., Anisuzzaman, S.M., 2015. Antioxidant activity and total phenolic content of an isolated *Morinda citrifolia* L. methanolic extract from Poly-ethersulphone (PES) membrane separator. *J. King Saud Univ.-Eng. Sci.* 27 (1), 63–67.
- Lee, P.I., Hsueh, P.R., 2020. Emerging threats from zoonotic coronaviruses—from SARS and MERS to 2019-nCoV. *J. Microbiol. Immunol. Infect.* 53 (3), 365.
- Liu, X., Zhang, B., Jin, Z., Yang, H., Rao, Z. 2020. The crystal structure of COVID-19 main protease in complex with an inhibitor N3. *Protein DataBank*.
- Mak, Y.W., Chuah, L.O., Ahmad, R., Bhat, R., 2013. Antioxidant and antibacterial activities of hibiscus (*Hibiscus rosa-sinensis* L.) and Cassia (*Senna bicapsularis* L.) flower extracts. *J. King Saud Univ. Sci.* 25 (4), 275–282.
- Olowa, L.F., Nuñez, O.M., 2013. Brine shrimp lethality assay of the ethanolic extracts of three selected species of medicinal plants from Iligan City, Philippines. *Int. Res. J. Biol. Sci.* 2 (11), 74–77.
- Patel, K., Kumar, V., Rahman, M., Verma, A., Patel, D.K., 2018. New insights into the medicinal importance, physiological functions, and bioanalytical aspects of an important bioactive compound of foods 'Hyperin': Health benefits of the past, the present, the future. *Beni-Suef Univ. J. Basic Appl. Sci.* 7 (1), 31–42.
- Pavić, K., Perković, I., Gilja, P., Kozlina, F., Ester, K., Kralj, M., Schols, D., Hadjipavlou-Litina, D., Pontiki, E., Zorc, B., 2016. Design, synthesis, and biological evaluation of novel primaquine-cinnamic acid conjugates of the amide and acylsemicarbazide type. *Molecules* 21 (12), 1629.
- Pisoschi, A.M., Negulescu, G.P., 2011. Methods for total antioxidant activity determination: a review. *Biochem. Anal. Biochem.* 1 (1), 106.
- Qi, S.H., Miao, L., Gao, C.H., Xu, Y., Zhang, S., Qian, P.Y., 2010. New steroids and a new alkaloid from the gorgonian *Isis minorbrachyblasta*: structures, cytotoxicity, and antilarval activity. *Helv. Chim. Acta* 93 (3), 511–516.
- Shoker, R.M., 2020. A Review Article: The importance of the major groups of plants secondary metabolism phenols, alkaloids, and terpenes. *Int. J. Res. Appl. Sci. Biotechnol.* 7 (5), 354–358.
- Šircelj, H., Mikulič-Petkovšek, M., Batič, F., 2010. Antioxidants in spring leaves of *Oxalis acetosella* L. *Food Chem.* 123 (2), 351–357.
- Supraja, N., Prasad, T.N.V.K.V., Gandhi, A.D., Anbumani, D., Kavitha, P., Babujanarthanam, R., 2018. Synthesis, characterization and evaluation of antimicrobial efficacy and brine shrimp lethality assay of *Alstonia scholaris* stem bark extract mediated ZnONPs. *Biochem. Biophys. Res.* 14, 69–77.
- Uma, C., Sekar, K.G., 2014. Phytochemical analysis of a folklore medicinal plant *Citrullus colocynthis* L (bitter apple). *J. Pharmacogn. Phytochem.* 2 (6).
- Uzayisenga, R., Ayeka, P.A., Wang, Y., 2014. Anti-diabetic potential of *Panax notoginseng* saponins (PNS): a review. *Phytother. Res.* 28 (4), 510–516.
- Xu, X., Chen, P., Wang, J., Feng, J., Zhou, H., Li, X., 2020. Evolution of the novel coronavirus from the ongoing Wuhan outbreak and modeling of its spike protein for risk of human transmission. *Sci. China Life Sci.* 63, 457–460.
- Zahra, S.A., Iqbal, J., Abbasi, B.A., Shahbaz, A., Kanwal, S., Shah, S.L., Ahmad, P., Mahmood, T., 2021. Antimicrobial, cytotoxic, antioxidants, enzyme inhibition activities, and scanning electron microscopy of *Lactuca orientalis* (Boiss.) Boiss. seeds. *Microsc. Res. Tech.* 84 (6), 1284–1295.
- Zhao, L., Yuan, X., Wang, J., Feng, Y., Ji, F., Li, Z., Bian, J., 2019. A review on flavones targeting serine/threonine protein kinases for potential anticancer drugs. *Bioorg. Med. Chem.* 27 (5), 677–685.